Biophysical Journal Volume 88 March 2005 1809–1817

Trapping Crystal Nucleation of Cholesterol Monohydrate: Relevance to Pathological Crystallization

Inna Solomonov,* Markus J. Weygand,† Kristian Kjaer,† Hanna Rapaport,‡ and Leslie Leiserowitz*

*Department of Materials and Interfaces, The Weizmann Institute of Science, 76100 Rehovot, Israel; †Materials Research Department, Risø National Research Laboratory, 4000 Roskilde, Denmark; and ‡Department of Biotechnology Engineering, Ben-Gurion University of the Negev, 84105 Beer-Sheva, Israel

ABSTRACT Crystalline nucleation of cholesterol at the air-water interface has been studied via grazing incidence x-ray diffraction using synchrotron radiation. The various stages of cholesterol molecular assembly from monolayer to three bilayers incorporating interleaving hydrogen-bonded water layers in a monoclinic cholesterol·H_2O phase, has been monitored and their structures characterized to near atomic resolution. Crystallographic evidence is presented that this multilayer phase is similar to that of a reported metastable cholesterol phase of undetermined structure obtained from bile before transformation to the triclinic phase of cholesterol·H_2O, the thermodynamically stable macroscopic form. According to grazing incidence x-ray diffraction measurements and crystallographic data, a transformation from the monoclinic film structure to a multilayer of the stable monohydrate phase involves, at least initially, an intralayer cholesterol rearrangement in a single-crystal-to-single-crystal transition. The preferred nucleation of the monoclinic phase of cholesterol·H_2O followed by transformation to the stable monohydrate phase may be associated with an energetically more stable cholesterol bilayer arrangement of the former and a more favorable hydrogen-bonding arrangement of the latter. The relevance of this nucleation process of cholesterol monohydrate to pathological crystallization of cholesterol from cell biomembranes is discussed.

INTRODUCTION

Abnormally high physiological levels of cholesterol may precipitate into crystallites that appear in atherosclerotic plaques (Small and Shipley, 1974; Small, 1998; Guo et al., 2000), in gallstones (Bogren and Larsen, 1963), and cataractous eye lenses (Jacob et al., 2001).

Cholesterol crystallization from cultured foam cells (Kellner-Welbel et al., 1999) displayed various morphologies that included needles, helices, and plates, in which the quantity of the latter increased with time. Various studies on cholesterol crystallization in model or native bile solutions by light, electron microscopy, and x-ray diffraction (Kaplun et al., 1994; Somjen et al., 1995; Wang and Carey, 1996) have provided evidence that crystallites form through aggregation of cholesterol-rich vesicles. Konikoff, Talmon, and co-workers, in a study of cholesterol crystallization from bile, had detected by cryotransmission electron microscopy (cryo-TEM) that edges of early-formed cholesterol crystals were lined up with micelles and multilamellar vesicles (Konikoff et al., 2000). Furthermore, Carey and co-workers (Konikoff et al., 1992) had obtained an x-ray powder diffraction pattern from early-formed filamentous crystallites of cholesterol in bile solution that was interpreted as depicting an unknown crystalline polymorph of cholesterol, before transformation to plates of the stable monohydrate phase. This crystallization process is similar to that described above from cultured foam cells (Kellner-Welbel et al., 1999).

In a study aimed at monitoring the early stages of crystallization of cholesterol at the air-water interface via grazing incidence x-ray diffraction (GIXD) using synchrotron radiation, we had found that cholesterol crystallizes on water in mono- and bilayer form in phases (Lafont et al., 1998; Rapaport et al., 2001) different from the known three-dimensional (3D) cholesterol crystal structures. The GIXD patterns of the cholesterol films displayed a broad Bragg peak for the film in the uncompressed state, and several sharp Bragg peaks upon compression of the film well beyond monolayer collapse. The broad Bragg peak arises from a cholesterol monolayer embodying poorly ordered two-dimensional crystalline domains, each containing ~200 molecules in a proposed trigonal arrangement. The sharp Bragg peaks correspond to a rectangular unit cell $a = 10.07$ Å, $b = 7.57$ Å, in a crystalline bilayer with an average domain size of ~5000 molecules. X-ray reflectivity measurements of the film on water revealed a disordered cholesterol layer lying above the crystalline bilayer. With time this triple-layered phase underwent a partial transformation into a crystalline trilayer with a structure akin to that of the 3D triclinic crystal of cholesterol monohydrate (Craven, 1976).

The 10×7.5 Å^2 layer motif is adopted in crystal structures of cholesterol-type molecules in monolayer, multilayer, and macroscopic form (Table 1 in Supplementary Material), as well as in the 3D crystals of several steroid-type molecules according to their unit cell dimensions (Bernal et al., 1940). Thus, a question may be posed as to why cholesterol does not adopt the 10×7.5 Å^2 bilayer motif in a stable macroscopic hydrate phase. We had not obtained a multilayer of the 10×7.5 Å^2 motif from a film of pure cholesterol on the water

Submitted April 22, 2004, and accepted for publication November 23, 2004.

Address reprint requests to Leslie Leiserowitz, E-mail: leslie.leiserowitz@weizmann.ac.il.

0006-3495/05/03/1809/09 $2.00

doi: 10.1529/biophysj.104.044834

surface. Nevertheless, solid solutions of cholesterol and stigmasterol in the molar range 25:75–65:35 did yield a multilayer structure (I. Solomonov, H. Kjaer, H. Rapaport, and L. Leiserowitz, unpublished data). Furthermore, we belatedly recognized that GIXD data from a compressed film of a 5:1 mixture of cholesterol/dipalmitoyl phosphatidylcholine (DPPC), but which yielded very weak Bragg rod intensity profiles and thus had not been included in the article by Lafont et al. (1998), suggested the presence of a cholesterol crystalline phase adopting the 10×7.5 Å^2 motif about three layers thick. These results provided incentive for obtaining multilayer crystals of cholesterol adopting the 10×7.5 Å^2 motif, particularly when making use of mixtures with phospholipids.

Here we report first a GIXD study of a compressed film of pure cholesterol on water, comprising crystallites of the 10×7.5 Å^2 bilayer and a multilayer in high yield of the stable triclinic monohydrate phase that incorporates a 12.4×12.4 Å^2 bilayer motif. We next discuss two 5:1 mixtures of cholesterol with phospholipids dimyristoyl phosphatidylcholine (DMPC) and DPPC on water, which formed films of different thickness of the same crystalline phase. An x-ray structure determination to near atomic resolution from these mixtures revealed a cholesterol monohydrate phase incorporating the 10×7.5 Å^2 bilayer motif interlinked via ordered water to form films 2–3 bilayers thick. Evidence is given that this multilayer phase is similar in structure to that of the metastable filaments of cholesterol from bile (Konikoff et al., 1992), as well as to a metastable cholesterol phase also obtained from bile examined by cryoelectron diffraction and lattice imaging microscopy (Weihs et al, 2005). Finally, a structural model of the transition from the 10×7.5 Å^2 bilayer motif to the macroscopic stable monohydrate phase is presented.

MATERIALS AND METHODS

Cholesterol and two phospholipids, DPPC and DMPC of the highest purity available, obtained from Sigma (St. Louis, MO). Lipid/chloroform solutions (~0.1 mg/ml) were used to form the monolayer films at the air-water interface for surface pressure-molecular area isotherms and GIXD measurements.

A detailed description of GIXD applied to films on liquid surfaces has been given elsewhere (Als-Nielsen and Kjaer, 1989; Kuzmenko et al., 2001). The GIXD experiments described here were performed on the liquid surface diffractometer at the undulator BW1 beam line at the HASYLAB synchrotron source (Deutsches Elektronen-Synchrotron, Hamburg, Germany). The films were spread in an open trough on the water surface in a homogeneous manner at room temperature. The air in the closed trough was replaced by helium to reduce x-ray background scattering. The x-ray diffraction measurements were performed with the water subphase cooled to 5°C. A monochromatic x-ray beam ($\lambda = 1.304$ Å) was adjusted to strike the liquid surface at an incident angle $\alpha_i < 0.85\alpha_c$, where α_c is the critical angle for total external reflection; this maximizes surface sensitivity. The GIXD signals are obtained from thin film crystallites that are randomly oriented about the water surface normal in the form of a two-dimensional ''powder''. Details on GIXD as applied to the crystalline films reported here and on the method of x-ray structure determination of the multilayer of cholesterol are presented in the Supplementary Material.

RESULTS

Mixture of the 10×7.5 Å^2 bilayer and the 12.4×12.4 Å^2 multilayer phase of cholesterol

Pure cholesterol deposited on the water surface to form a monolayer film and compressed in a continuous manner to a nominal area of 16 Å^2/molecule yielded a GIXD pattern (Fig. 1) that arises from a mixture of the rectangular 10×7.5 Å^2 bilayer phase and a multilayer of the triclinic monohydrate phase that incorporates the 12.4×12.4 Å^2 bilayer motif (Craven, 1976). (A similar GIXD pattern was obtained without cooling the aqueous subphase to 5°C.) The unit cell dimensions of the rectangular (a_r,b_r) and triclinic (a_t,b_t) phases determined from the q_{xy} positions of their q_z-integrated Bragg rods (denoted hereafter as Bragg peaks) (Fig. 1 *A*) and their assigned $\{h,k\}$ indices, yielded $a_r = 10.14$ Å, $b_r = 7.54$ Å, and $a_t = b_t = 12.38$ Å, $\gamma_t = 100.8°$, the latter set is very close to the reported values of the 3D crystal of the triclinic monohydrate form. The full width at half

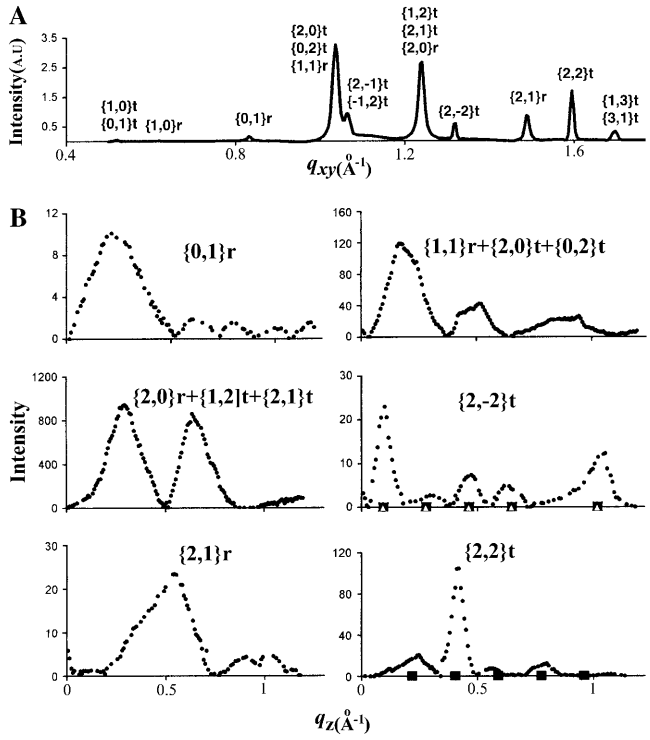

FIGURE 1 GIXD pattern of compressed film of pure cholesterol on water. (*A*) Bragg peak profiles $I(q_{xy})$. (*B*) Corresponding Bragg rod profiles $I(q_z)$. Reflection indices $\{h,k\}_r$ refer to the cholesterol bilayer in the rectangular 10×7.5 Å^2 unit cell; $\{h,k\}_t$ refer to the multilayer of the cholesterol triclinic monohydrate phase in the 12.4×12.4 Å^2 unit cell. The calculated positions along q_z of the individual intensity maxima of the $\{h,k,l\}_t$ reflections, namely $(h,k,l)_t$ and $(-h,-k,l)_t$, for the $\{2,2\}_t$ and $\{2,-2\}_t$ Bragg rods, are specified (*squares* and *triangles*). These positions are based on the known unit cell of the triclinic monohydrate phase (Craven, 1976). The curly brackets of the Bragg rod $\{h,k\}$ represent the overlapping Bragg rods $(h,k,+q_z)$ and $(-h,-k,+q_z)$, and in the case of rectangular *a*,*b* lattice the additional pair $(h,-k,+q_z)$ and $(-h,k,+q_z)$.

maximum (FWHM) along q_z of the intensity maxima of the $\{0,1\}_r$, $\{2,0\}_r$, and $\{2,1\}_r$ Bragg rods (Fig. 1 *B*) of the 10×7.5 Å^2 unit cell, yield a film thickness ($0.9 \times 2\pi$/FWHM) of ~30 Å, corresponding to a cholesterol bilayer as determined in an earlier GIXD study (Rapaport et al., 2001). The positions along q_z of the intensity maxima of the $\{2,-2\}_t$ and $\{2,2\}_t$ Bragg rods (Fig. 1 *B*) fit those calculated for the $\{2,-2,l\}$ and $\{2,2,l\}$ reflections of the macroscopic triclinic monohydrate phase. The FWHM of these intensity maxima yield a film thickness of 94 Å. This crystalline multilayer does not have a structure exactly identical to the macroscopic 3D form of cholesterol monohydrate (Craven, 1976) because the GIXD pattern (Fig. 1 *A*) exhibits weak $\{1,3\}_t$ and $\{3,1\}_t$ Bragg rods, whereas the corresponding $\{1,3,l\}$ and $\{3,1,l\}$ reflections in the 3D crystal are unobserved.

The Bragg peaks at $q_{xy} = 1.04$ Å^{-1} and 1.24 Å^{-1} (Fig. 1 *A*) each arise from a mixture of both phases. These Bragg peaks appear to be singlets suggesting a precise structural relationship between the two phases. Fig. 2 shows that the pertinent reciprocal vectors of the two phases are not parallel to each other.

Unit cell constants of a crystalline monoclinic phase of cholesterol in multilayer form

A 5:1 cholesterol/DPPC mixture deposited on the water surface to form a monolayer film and compressed in a continuous manner to surface pressure of 42 mN/M, corresponding to a nominal area of 11 Å^2/molecule, yielded a set of Bragg $\{h,k\}$ peaks (Fig. 3 *A*) characteristic of the cholesterol bilayer motif in the rectangular 10×7.5 Å^2 unit cell. A measure of the thickness of the crystalline film of 86 Å was gleaned from the average FWHM along q_z of the Bragg rod intensity maxima (Fig. 3 *B*) of 0.066 Å^{-1}. This latter value

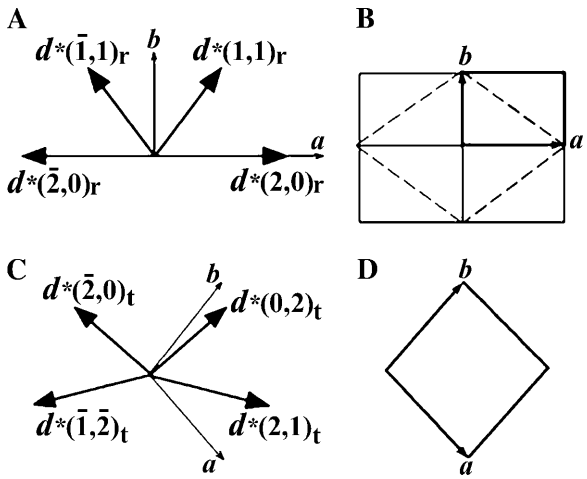

FIGURE 2 Geometric relationship between particular reciprocal lattice vectors and unit cell axes of cholesterol in: (*A*, *B*) the rectangular 10×7.5 Å^2 bilayer crystal; (*C*, *D*) the triclinic 12.4×12.4 Å^2 bilayer form of the multilayer crystal.

is about three times smaller than the FWHM (0.19 Å^{-1}) of the Bragg rod intensity maxima of the cholesterol bilayer film (Rapaport et al., 2001) whose thickness of 30 Å was independently determined by x-ray structure refinement. This comparison suggests that the cholesterol crystalline film is three bilayers thick. This ordered stack of three bilayers is consistent with the large number of regularly spaced intensity maxima along q_z of the Bragg rods (Fig. 3 *B*).

It proved possible to assign $\{h,k,l\}$ indices to all the intensity maxima along q_z in Fig. 3 *B*, consistent with treating the Bragg rods as arising from a 3D crystal of monoclinic symmetry with unit cell dimensions $a = 10.15(2)$ Å, $b = 7.57(2)$ Å, $c = 68.2(3)$ Å, $\beta = 94.8(5)°$, determined by a least-squares procedure (Table 2 in Supplementary Material). The calculated positions along q_z of the $\{h,k,l\}$ Bragg reflections are indicated in Fig. 3 *B*. The *h,k,l* indices of all the observed reflections obey the general condition $k + l = 2n$, implying a monoclinic *A*-centered unit cell. Such a cell may embody either of the space groups *Am*, *Aa*, *A*2/*m*, *A*2/*a*, or *A*2. Only *A*2 (the abbreviated version of *A*121) is allowed because naturally occurring cholesterol is a chiral molecule of one-handedness. Moreover, the *a* glide, as in *Aa* or *A*2/*a*, imposes the condition that *h*0*l* reflections must be absent for *h* odd, which is not satisfied because the 10*l* Bragg rod is present (Fig. 3). Thus, even pseudo-*a*-glide symmetry is precluded. Space group *A*2 incorporates rows of 2- and 2_1-axes parallel to *b*, alternating along the *c* axis, which is consistent with the symmetry of cholesterol bilayers in the crystal structures listed in Table 1 (Supplementary Material), which are formed via 2- or 2_1-symmetry, primarily the latter.

The monolayer film of the 5:1 cholesterol/DMPC mixture compressed to a surface pressure of 47 mN/M, corresponding to a calculated nominal area of 11 Å^2/molecule, yielded a GIXD pattern (vide infra) similar to that obtained from the DPPC mixture, but with fewer and less well-resolved Bragg rod intensity maxima. Thus, we focused on the Bragg rods from the 5:1 cholesterol/DPPC mixture for structure elucidation of the multilayer crystal.

Crystal structure determination of the cholesterol monoclinic phase in multilayer form

The integrated intensities of the Bragg rod $\{h,k,l\}$ intensity maxima were treated for structure determination as regular reflections arising from a 3D crystal. The Bragg rod data (Fig. 3 *B*) yielded 48 reflections of which 11 incorporate pronounced overlap between $(2,k,l)$ and $(-2,k,l+2)$ reflections. The crystal structure was determined to near atomic resolution via a constrained least-squares x-ray structure-factor refinement using SHELX software (Sheldrick, 1997).

For construction of a starting molecular model we considered the 3D crystal structures of cholesteryl myristate (Craven and de Titta, 1976), cholesteryl bromoheptadecanoate (Abrahamsson and Dahlen, 1977), and the cholesterol bilayer phase on water (Rapaport et al., 2001), all of which

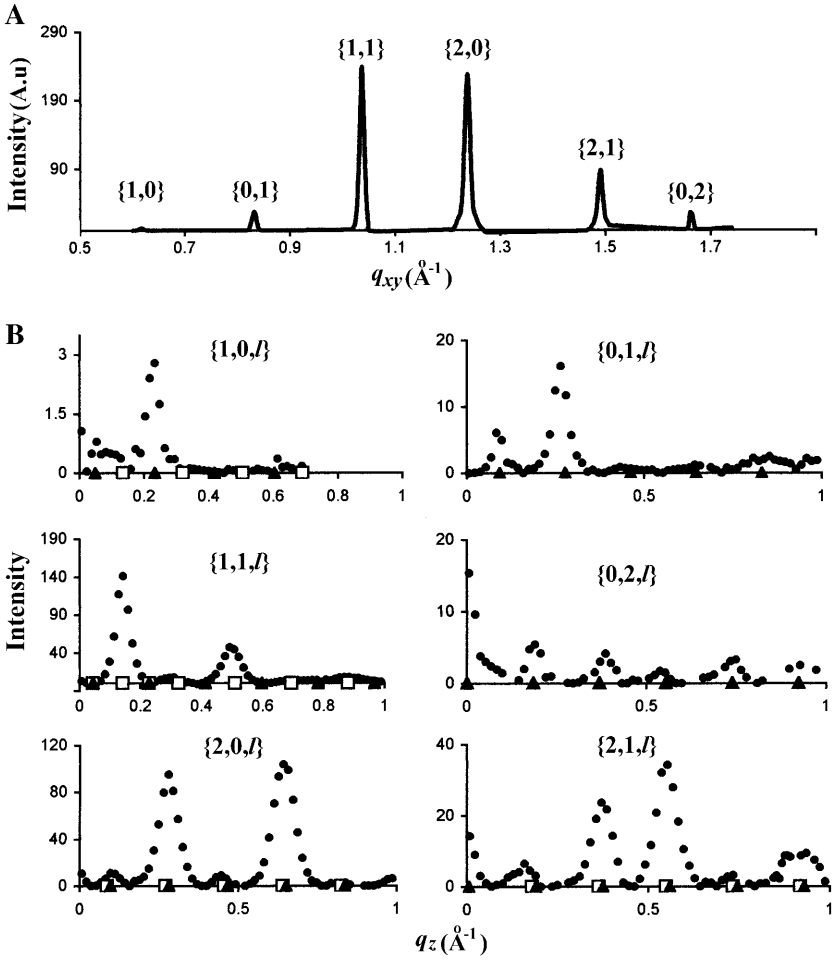

FIGURE 3 GIXD pattern of a compressed film of the 5:1 cholesterol/DPPC mixture on water. (*A*) The Bragg peak profiles $I(q_{xy})$. (*B*) The intensity profiles $I(q_z)$ of the corresponding Bragg rods. The calculated positions along q_z of the intensity maxima of the $\{h,k\}$ Bragg rods assuming they correspond to $\{h,k,l\}$ reflections of the monoclinic *A*2 unit cell are marked by triangles and squares. There is pronounced overlap between the $2,k,l$ and $-2,k,l + 2$ reflections (denoted by *triangles* and *squares*, respectively) along the {2,1} and {2,0} Bragg rods. The method of deriving the q_z values is described in Supplementary Material.

incorporate the 10 × 7.5 Å^2 bilayer motif. We did not include the anhydrous crystalline form of cholesterol; even though its unit cell dimensions (Table 1 in Supplementary Material) appear to correspond to a supercell of the 10 × 7.5 Å^2 motif, its layer arrangement is different. Furthermore, the surface of the bilayer of anhydrous cholesterol is highly corrugated and thus the lattice energy of such a bilayer is less stable than that of the flat bilayer and would be unfavorable on a flat water surface. The three structures considered have similar unit cell areas per molecule in the *ab* plane of 39.0 Å^2, 39.5 Å^2, and 38.1 Å^2, with a corresponding bilayer thickness, defined as the distance between the hydroxyl O atoms at opposite sides of the bilayer of 32.9 Å, 32.8 Å, and 29.5 Å[1], respectively. The cholesterol bilayer on water obviously has too low a thickness, in all probability a result of incomplete x-ray structure refinement and was thus excluded. In view of the similar intralayer motifs of the other two cholesteryl derivates, the layer structure of cholesteryl myristate was chosen as our starting model.

There were essentially two distinct structural unknowns: the offset in the *x*-direction between the neighboring cholesterol layers forming the bilayer and the symmetry thereof, because the bilayer may be generated via twofold or twofold screw symmetry. The offset was determined by a stepwise variation of the layer structure along *x* so as to obtain the best fit between observed and calculated x-ray structure factors for the $\{1,0,l\}$ and $\{2,0,l\}$ reflections. Next, we determined the symmetry element relating neighboring bilayers, by employing the four models (1–4) shown schematically in Fig. 9 (Supplementary Material). A meaningful x-ray structure-factor refinement of each model is possible only if constraints are imposed on the cholesterol molecular structure in view of the limited number (48) of ''observed reflections''. Thus the four models were refined by x-ray structure-factor computations allowing the two molecules in the crystal asymmetric unit (Fig. 9, *A* and *B*, in Supplementary Material) to move as independent rigid bodies. This constraint resulted in a total of 12 parameters to yield reliability factors *R*, on the basis of which models 2 and 4 could be discarded.

The next stage involved determination of the water structure in models 1 and 3. The space of ~2 Å between neighboring cholesterol bilayers in the two models is appropriate for insertion of an interleaving monohydrate

water layer because the corresponding value in the 3D crystal structure of the cholesterol monohydrate triclinic phase (Craven, 1976) is 1.5 Å. In models 1 and 3, the cholesterol layers sandwiching the proposed interleaving water layer are related by twofold screw (2_1) and twofold (2) symmetry, respectively (Fig. 9, *A* and *C*, in Supplementary Material). A reasonable hydrogen-bonding arrangement involving the sterol hydroxyl groups and water molecules as a monohydrate phase could only be constructed for model 1. We were not able for model 3 to generate a favorable hydrogen-bonding bilayer arrangement, formed via twofold symmetry along the *b* axis, and that incorporated the positions of refined sterol O atoms and inserted water molecules. Further refinement of model 1, keeping the water oxygen atoms fixed in their inserted positions, yielded an *R*-factor, $\Sigma||F_{obs}|^2 - |F_{calc}|^2|/\Sigma|F_{obs}|^2$, of 13.5%. The observed and calculated $|F(h,k,l)|^2$ values are shown in Fig. 4 and the molecular packing arrangement and hydrogen-bond motif in Fig. 5. The refined *x*, *y*, *z* coordinates of model 1 are listed in Table 4, Supplementary Material.

Monitoring the initial growth of the monoclinic cholesterol·H_2O phase by GIXD

Monitoring the growth from inception of a molecular crystal layer-by-layer via x-ray (or neutron) diffraction has been a challenge in the study of crystal nucleation. Here we demonstrate the feasibility of such an approach, but indirectly, by a GIXD ''snapshot'' technique involving the measurement of Bragg rods of different cholesterol crystalline films, containing approximately one, two, and three 10 × 7.5 $Å^2$ bilayers, respectively. The Bragg rod data from the crystalline 10 × 7.5 $Å^2$ bilayer of cholesterol (Rapaport et al., 2001) are displayed in Fig. 6 *A*. The corresponding Bragg rods of the compressed film of the 5:1 cholesterol/DPMC mixture (Fig. 6 *B*) is indicative of a cholesterol crystalline film ~55-Å thick according to the average FWHM of the Bragg rod intensity maxima, and thus contains almost two bilayers. As discussed above, the FWHM of the intensity maxima along the Bragg rods from the 5:1 cholesterol/DPPC mixture (Fig. 6 *C*), corresponds to a monoclinic crystalline cholesterol monohydrate phase about three bilayers thick.

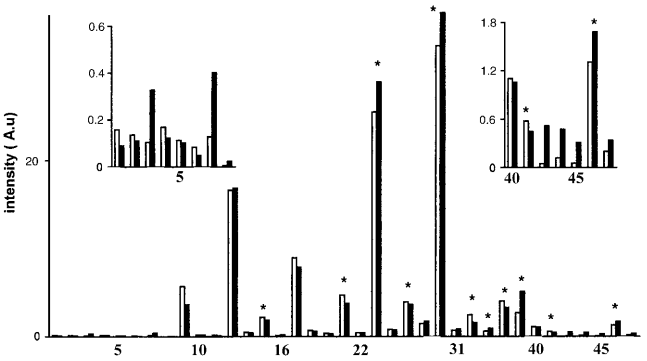

FIGURE 4 The observed (*soild bars*) and calculated (*open bars*) values of the x-ray structure factors $|F(h,k,l)|^2$, the latter based on the structural model of the monoclinic *A*2 phase of cholesterol monohydrate. The $|F(h,k,l)|^2$ values are displayed as a function of increasing $q(h,k,l)$, equally separated for clarity of presentation. The bars marked with an asterisk, represent reflection pairs of the type $(2,k,l)$ and $(-2,k,l+2)$, which are heavily overlapped in the GIXD pattern (see Fig. 3 *B*) and thus are shown superimposed. The observed and calculated $|F(h,k,l)|^2$ are listed in Supplementary Material.

DISCUSSION

The monoclinic and triclinic phases of cholesterol·H_2O in multilayer form

Highly compressed pure cholesterol on water yielded a triple bilayer, incorporating the 12.4 × 12.4 $Å^2$ bilayer motif, corresponding to the thermodynamically stable triclinic cholesterol·H_2O phase, as well as a bilayer of the 10 × 7.5 $Å^2$ motif, whereas a less-compressed film of pure cholesterol had yielded only one bilayer of the 10 × 7.5 $Å^2$ motif (Rapaport et al., 2001). The highly compressed films of cholesterol in 5:1 mixtures with DMPC or DPPC form cholesterol crystalline films containing about two and three 10 × 7.5 $Å^2$ bilayers, respectively. The even number of bilayers formed in all cases suggest that the crystal nuclei tend to increase in thickness in bilayer form, consistent with growth experiments on macroscopic-size crystals of cholesterol·H_2O monitored by atomic and chemical force microscopy (Abendan and Swift, 2002). This tendency is probably driven by the interlayer contacts involving the exocyclic groups that are disordered in crystalline cholesterol monolayers on water (Rapaport et al., 2001).

The structure of the crystalline cholesterol·H_2O film about three bilayers thick, obtained from the cholesterol/DPPC mixture, was determined to near atomic resolution. This structure (Fig. 5), of space group symmetry *A*2, comprises the 10 × 7.5 $Å^2$ cholesterol layers that form, via twofold symmetry, bilayers involving contact between flexible exocyclic moieties. Neighboring cholesterol bilayers, which are related by twofold screw symmetry, are interlinked by O-H···O hydrogen bonds involving the sterol OH groups and an ordered water layer (Fig. 5 *C*) to generate the multilayer film.

The molecular packing arrangements in the crystalline films of cholesterol containing the two and three 10 × 7.5 $Å^2$ cholesterol bilayers are the same in view of their very similar Bragg rods (Fig. 6, *B* and *C*), which indicates the presence of an interleaving ordered water layer already on formation of the second bilayer. In a similar way, ordered water layers interleave cholesterol bilayers adopting the 12.4 × 12.4 $Å^2$ motif in the triple-bilayer structure of cholesterol·H_2O, which is akin to that of the thermodynamically stable triclinic cholesterol·H_2O phase.

The preponderance of the 10 × 7.5 $Å^2$ bilayer in the crystal structures of various cholesterol-type molecules

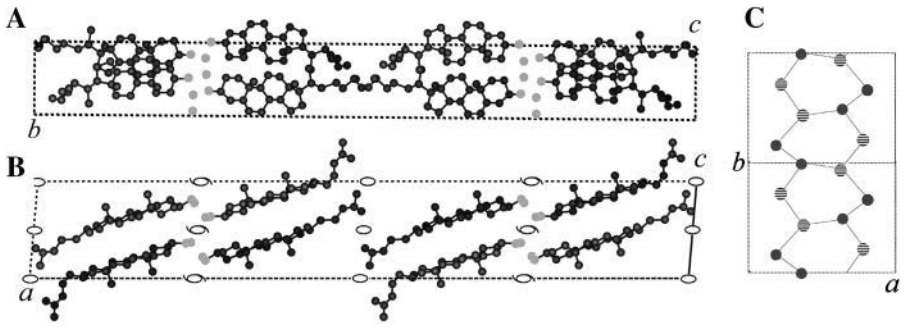

FIGURE 5 (*A*, *B*) Packing arrangement of the multilayer monoclinic *A*2 phase of cholesterol monohydrate depicting a ''complete unit cell'', as viewed along the *a* and *b* axes. The 2- and 2_1-axes are depicted in panel *B*. (*C*) Hydrogen-bonding arrangement at $z = 0.25$ viewed along a direction perpendicular to the *a*,*b* plane. The sterol and the water O atoms are colored gray and striped gray, respectively. Note that the hydrogen bond between the sterol O atoms of neighboring layers has a reasonable O···O distance of 2.9 Å that was not imposed in the x-ray structure refinement.

(Table 1 in Supplementary Material) indicates that this motif is preferred over the 12.4 × 12.4 Å^2 bilayer arrangement found in the triclinic cholesterol·H_2O phase. This observation is not inconsistent with their intralayer arrangements; the axially oriented methyl groups that emerge from the steroid plane appear to mesh more favorably in the 10 × 7.5 Å^2 motif (Fig. 7, *top left*) than in the 12.4 × 12.4 Å^2 motif (Fig. 7, *top right*). These observations imply that the hydrogen-bonding arrangement in the triclinic (12.4 × 12.4 Å^2) form must be the more stable, as appears to be the case: in the triclinic phase each oxygen atom participates in three hydrogen bonds in an extended network (Fig. 10 in Supplementary Material), whereas in the monoclinic phase half of the number of oxygen atoms participate in three hydrogen bonds and the remaining half form two hydrogen bonds, generating a ribbon network (Fig. 5 *C*).

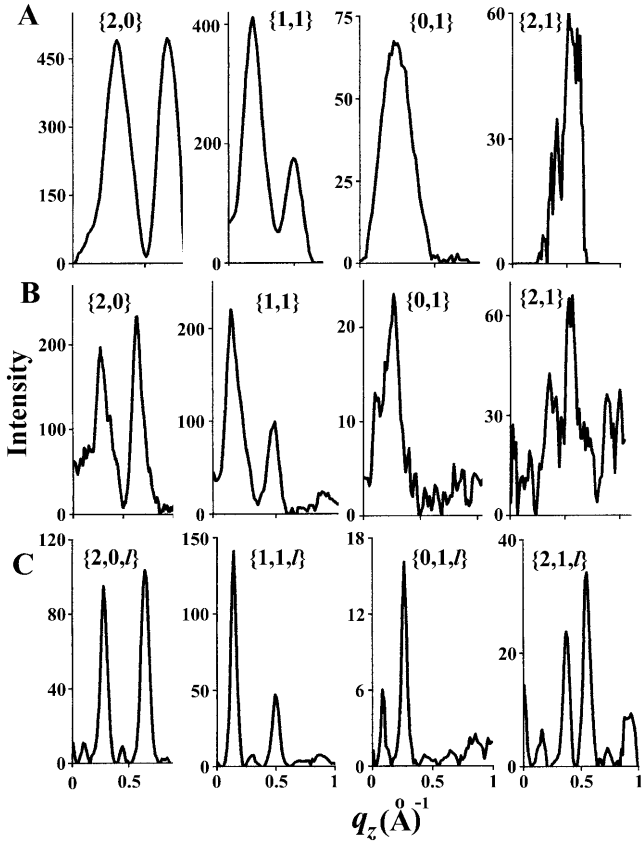

FIGURE 6 Bragg rods of three different compressed films on water of: (*A*) pure cholesterol, (*B*, *C*) 5:1 mixtures of cholesterol with phospholipids DMPC and DPPC, respectively. The relative intensities of the three films is not a measure of relative crystallinity, but rather reflects different measuring conditions. The single bilayer was obtained by compressing, but not continuously, a pure cholesterol film to a nominal area of 17 Å^2/molecule (Rapaport et al., 2001). The double and triple cholesterol bilayers were obtained by compressing, in a continuous manner, the film to a nominal area of ~11 Å^2/molecule.

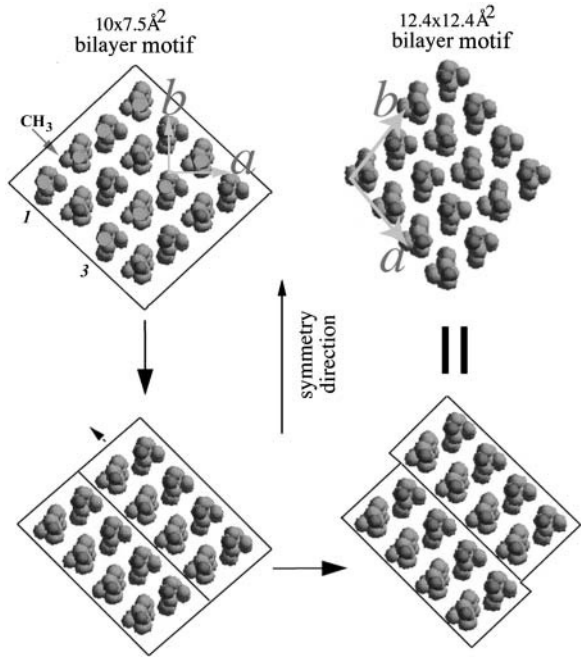

FIGURE 7 Model of an intralayer cholesterol transition from the rectangular 10 × 7.6 Å^2 bilayer motif to the 12.4 × 12.4 Å^2 bilayer in the triclinic monohydrate phase. Both layer structures are viewed down their long molecular axes. The first step of the transition involves a 180° rotation about their long axes of all molecules in alternating rows parallel to the direction $a + b$, labeled 1 and 3. The second step involves a shift between molecular rows in the direction $-a + b$. The axially oriented methyl groups (CH_3), which superimpose, are indicated.

Similarity between the cholesterol monoclinic phase and the metastable phase from bile

The following evidence indicates that the monoclinic multilayer phase and the metastable filamentous phase of cholesterol (Konikoff et al., 1992) are similar. Their long lattice spacings, 34.0(1) and 34.1(1) Å, respectively, are equal in length. The calculated density of 1.029(5) g/mL of the multilayer phase, assuming the monohydrate structure, is very close to the measured density of the filamentous crystals (1.032 g/mL). The powder x-ray diffraction pattern of the filamentous phase (Fig. 8 *A*) in the range given, displays only two prominent Bragg peaks with *d*-spacings of 5.9 and 4.9 Å. These two reflections match well, both in *d*-spacing and relative intensity, the {111} ($d = 6.0$ Å) and {202} ($d = 4.9$ Å) peaks of the multilayer phase (Fig. 8 *B*). The latter, however, displays two additional strong reflections (115) ($d = 5.4$ Å) and (206) ($d = 4.5$ Å), respectively. Their absence in the powder pattern of the filamentous crystals may be rationalized by assuming the presence of interbilayer defects involving the water layer or that the bow-like shape of the filaments was sufficient to diminish intensities of the (*h,k,l*) reflections with higher *l* indices. It is noteworthy that the cholesterol multilayers on water were not bent, for such behavior would have incurred skewed Bragg rods (Kuzmenko et al., 2001).

The monoclinic phase of cholesterol·H_2O appears to be also very similar to that of lathe-like cholesterol crystals obtained from bile, studied by cryo-TEM images and cryoelectron diffraction patterns (Weihs et al., 2005). One cryoelectron diffraction pattern, which corresponds to a transient crystal form that lasted for several days, may be indexed according to the monoclinic cholesterol monohydrate phase to yield nonsatellite reflections of the type $\{h,k,l = h\}$ obeying the condition $k + l = 2n$ with overall *mm* symmetry and belonging to a 10×7.5 Å^2 unit cell. The pattern exhibits strong reflections {202} and {111} akin to those of the multilayer form of monoclinic cholesterol·H_2O.

Transition from the monoclinic to the triclinic phase of cholesterol·H_2O

The similarity in geometry as well as relative orientation of a subset of diffraction vectors belonging to the 10×7.5 Å^2 bilayer structure and the multilayer of the 12.4×12.4 Å^2 monohydrate phase (Fig. 2, *A* and *C*), lends credence to the model that a transformation from the monoclinic (10×7.5 Å^2) phase to the triclinic (12.4×12.4 Å^2) phase would involve a single-crystal-to-single-crystal molecular rearrangement.

Assuming this transition, the symmetry *b* axis of the 10×7.5 Å^2 bilayer phase would be converted into the pseudo-rotation axis along the diagonal $a - b$ of the 12.4×12.4 Å^2 bilayer phase (cf. Fig. 2, *B* and *D*). It is also noteworthy that in both bilayer structures the long axes of the cholesterol molecules are tilted from the layer normal by an angle of ~19°, in a plane perpendicular to the crystal (pseudo) symmetry axis. Thus, any transformation in one layer of the initial phase could, by symmetry, occur in an equivalent manner in an adjacent layer with the orientation of the long molecular axes left essentially unchanged. Another feature common to both structures lies in the similarity in length of the diagonals $a \pm b$ in the monoclinic phase (12.6 Å) and of the *a* and *b* axes in the triclinic phase (12.4 Å) (see Fig. 2, *B* and *D*). However, the precursor of the triclinic unit cell (Fig. 2 *B*, *dashed lines*) would undergo an angular distortion on transformation to the triclinic phase (Fig. 2 *D*), suggesting that the proposed transition from a macroscopic-sized crystal would occur only in the early stages. A model of the proposed intralayer cholesterol phase transition is depicted in Fig. 7.

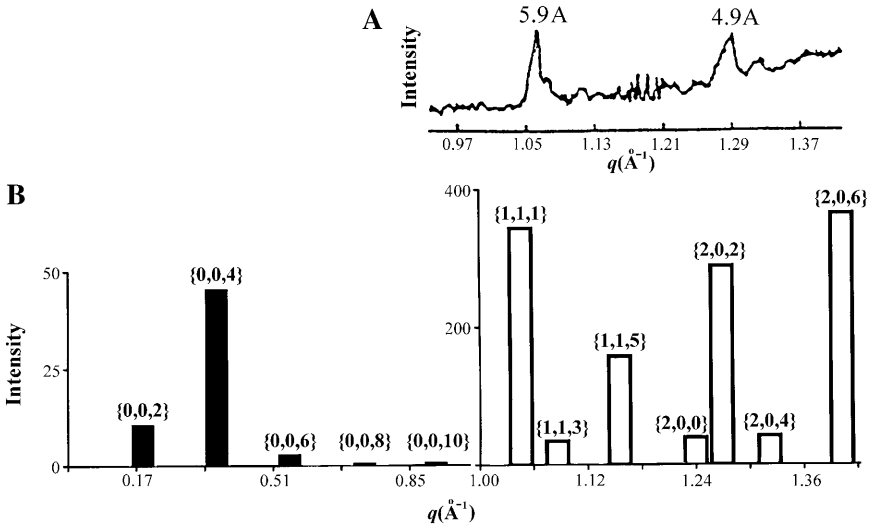

FIGURE 8 (*A*) Measured x-ray powder diffraction pattern of the filamentous phase of cholesterol from bile (Konikoff et al., 1992). The range in *q* of 0.91–1.43 Å^{-1} corresponds to $d\ (= 2\pi/q)$ spacings of 6.9–4.4 Å. (*B*) Simulated x-ray powder diffraction pattern of the monoclinic cholesterol·H_2O phase showing the strongest measured $|F(h,k,l)|^2$ values from the GIXD pattern (*open bars*) within a *q* range of 1.00–1.42 Å^{-1} as well as several calculated $|F(0,0,l)|^2$ values (*solid bars*) as derived from the crystal structure. These $|F(0,0,l)|^2$ reflections were not measured for technical reasons. Fig. 8 reproduced with permission from the Journal of Clinical Investigation.

This model, which requires a 180° rotation of half the number of molecules, is supported by an in situ observation, via polarization microscopy and Raman spectroscopy, of an epitaxial polymorphic transformation of a norethindrone analog, in which half the number of molecules would have to undergo a pronounced rotation (Boerrigter et al., 2002).

The interplay between intra- and interbilayer crystalline stability in determining the order of appearance of the two monohydrate forms of cholesterol, particularly as made manifest in the crystallization of cholesterol from bile, is supported by the crystalline dimorphic behavior of alkane $C_{24}H_{50}$ and of p-CH_3O-C_6H_4-CH=CH-CO_2H. In these systems, the less stable dimorph crystallizes, provided the nucleation starts layer by layer, because the intralayer arrangement of the less stable phase is the more energetically favorable (Weissbuch et al., 2003).

Model of the crystal nucleation process of cholesterol·H_2O from a biomembrane

It has been reported that the site of nucleation in atherosclerotic plaques may occur within the biomembrane (Kellner-Welbel et al., 1999). Cholesterol in a biomembrane would require a concentration large enough to phase separate into domains with an interlayer overlap sufficient to generate the crystalline 10×7.5 Å^2 bilayer. We may preclude nucleation of a bilayer with a structure akin to that of the anhydrous form of cholesterol (Shieh et al., 1977) because it would be highly corrugated and thus have a lattice energy less favorable than that of the 10×7.5 Å^2 bilayer motif, which has relatively flat surfaces. A cholesterol crystalline bilayer embedded in a model phospholipid-cholesterol bilayer membrane, the formation of which would depend on the cholesterol concentration and cholesterol-phospholipid interactions (McConnell and Radhakrishnan, 2003), has yet to be reported. Work along these lines is under way.

Concluding remarks

The study of crystal nucleation of cholesterol at the air-water interface by a grazing incidence x-ray diffraction ''snapshot'' technique not only has revealed information on pathological crystallization of cholesterol, it has also yielded insight into the general process of crystal nucleation.

SUPPLEMENTARY MATERIAL

An online supplement to this article can be found by visiting BJ Online at http://www.biophysj.org.

We thank Dr. Isabelle Weissbuch for assistance and advice and Prof. M. Lahav for discussions. We are indebted to HASYLAB for synchrotron beam time.

This work was supported by the Kimmelmann Center, the DanSync program of the Danish Natural Science Research Council, and the European Community under Training and Mobility of Researchers contract ERBFMGECT950059.

REFERENCES

Abendan, R. S., and J. A. Swift. 2002. Surface characterization of cholesterol monohydrate crystals by chemical force microscopy. *Langmuir*. 18:4847–4853.

Abrahamsson, S., and B. Dahlen. 1977. The crystal structure of cholesteryl 17-bromoheptadecanoate. *Chem. Phys. Lipids*. 20:43–56.

Als-Nielsen, J., and K. Kjaer. (1989). X-ray reflectivity and diffraction studies of liquid surfaces and surfactant monolayers. *In* Phase Transitions in Soft Condensed Matter. T. Riste and D. Sherrington, editors. Plenum Press, New York. 211:113–138.

Bernal, J. D., D. Crowfoot, and I. Fankuchen. 1940. X-ray crystallography and the chemistry of the steroids. *Philos. Trans. R. Soc. Lond. A*. 239: 135–182.

Boerrigter, S. X. M., C. J. M. van den Hoogenhof, H. Meekes, P. Bennema, and E. Vlieg. 2002. In-situ observation of epitaxial nucleation of the model steroid methyl analogue of norethindrone. *J. Phys. Chem. B*. 106:4725–4731.

Bogren, H., and K. Larsen. 1963. An x-ray diffraction study of crystalline cholesterol in some pathological deposits in man. *Biochim. Biophys. Acta*. 75:65–69.

Craven, B. M. 1976. Cholesterol monohydrate. *Nature*. 260:727–729.

Craven, B. M., and G. T. de Titta. 1976. Cholesteryl myristate: structure of the crystalline solids and mesophases. *J.C.S. Perkin*. 2:814–822.

Guo, W., J. Morrisett, M. DeBakey, G. Lawrie, and J. Hamilton. 2000. Quantification in situ of crystalline cholesterol and calcium phosphate hydroxyapatite in human atherosclerotic plaques by solid angle magic angle spinning NMR. *Arterioscler. Thromb. Vasc. Biol.* 20:1630–1636.

Jacob, R. F., R. J. Cenedella, and R. P. Mason. 2001. Evidence for distinct cholesterol domains in fiber cell membranes from cataractous human lenses. *J. Biol. Chem.* 276:13573–13578.

Kaplun, A., Y. Talmon, F. M. Konikoff, M. Rubin, A. Eitan, M. Tadmor, and D. Lichtenberg. 1994. Direct visualization of lipid aggregates in native human bile by light-transmission and cryo-transmission electron microscopy. *FEBS Lett.* 340:78–82.

Kellner-Welbel, G., P. G. Yancey, W. G. Jerome, T. Walser, R. P. Mason, M. C. Phillipis, and G. H. Rothblatt. 1999. Arteriosclerosis and cholesterol crystallization. *Arterioscler. Thromb. Vasc. Biol.* 19:1891–1898.

Konikoff, F. M., D. S. Chung, J. M. Donovan, D. M. Small, and M. C. Carey. 1992. Filamentous, helical and tubular microstructures during cholesterol crystallization from bile: evidence that cholesterol does not nucleate classic monohydrate plates. *J. Clin. Invest.* 90:1155–1160.

Konikoff, F., D. Danina, D. Weihs, M. Rubin, and Y. Talmon. 2000. Microstructural evolution of lipid aggregates in nucleating model and human bile visualized by cryogenic transmission electron microscopy. *Hepatology*. 31:261–268.

Kuzmenko, I., H. Rapaport, K. Kjaer, J. Als-Nielsen, I. Weissbuch, M. Lahav, and L. Leiserowitz. 2001. Design and characterization of crystalline thin film structures at the air-liquid interface: simplicity to complexity. *Chem. Rev.* 101:1659–1696.

Lafont, S., H. Rapaport, G. J. Somjen, A. Renault, P. B. Howes, K. Kjaer, J. Als-Nielsen, L. Leiserowitz, and M. Lahav. 1998. Monitoring the nucleation of crystalline films of cholesterol on water and in the presence of phospholipid. *J. Phys. Chem.* 102:761–765.

McConnell, H. M., and A. Radhakrishnan. 2003. Condensed complexes of cholesterol and phospholipids. *Biochim. Biophys. Acta*. 1610:159–173.

Rapaport, H., I. Kuzmenko, S. Lafont, K. Kjaer, P. B. Howes, J. Als-Nielsen, M. Lahav, and L. Leiserowitz. 2001. Cholesterol monohydrate nucleation in ultrathin films on water. *Biophys. J.* 81:2729–2736.

Sheldrick, G. M. 1997. SHELXL-97 Program for Crystal Structure Determination. University of Gottingen, Gottingen, Germany.

Shieh, H. S., L. G. Hoard, and C. E. Nordman. 1977. Crystal structure of anhydrous cholesterol. *Nature*. 267:287–289.

Small, D. M. 1998. Progression and regression of arteriosclerotic lesions: insight from lipid physical biochemistry. *Arteriosclerosis*. 8:103–129.

Small, D. M., and G. G. Shipley. 1974. Physical chemistry basis of lipid deposition arteriosclerosis. *Science*. 185:222–229.

Somjen, G. J., G. Lipka, G. Schulthess, M. H. J. Koch, E. Wachtel, T. Gilat, and H. Houser. 1995. Behavior of cholesterol and spin-labeled cholestane in model bile systems studied by electron spin resonance and synchrotron x-rays. *Biophys. J*. 68:2342–2349.

Wang, D., and M. C. Carey. 1996. Characterization of crystalline pathways during cholesterol precipitation from human gallbladder biles. Identical pathways to corresponding model biles with three predominating sequences. *J. Lipid Res*. 37:2539–2549.

Weihs, D., J. Schmidt, I. Goldiner, D. Danino, M. Rubin, Y. Talmon, and F. M. Konikoff. 2005. Biliary cholesterol crystallization characterized by single crystal Cryogenic-Electron Diffraction. *J. Lipid Res*. In press.

Weissbuch, I., M. Lahav, and L. Leiserowitz. 2003. Towards stereochemical control, monitoring and understanding of crystal nucleation. *Cryst. Growth Des*. 3:125–150.